

# Feedforward–Feedback Integration in Flight Control: Reinforcement Learning with Sliding Mode Control

Imran Sayyed

Indian Institute of Technology Madras, Chennai, 600036, India

Nandan Kumar Sinha

Indian Institute of Technology Madras, Chennai, 600036, India

**Abstract**— Learning-based controllers leverage nonlinear couplings and enhance transients but seldom offer guarantees under tight input constraints. Robust feedback like sliding-mode control (SMC) provides these guarantees but is conservative in isolation. This paper creates a learning-augmented framework where a deep reinforcement learning policy produces feedforward commands and an SMC law imposes actuator limits, bounds learned authority, and guarantees robustness. The policy is modeled as a matched, bounded input, and Lyapunov-based conditions link SMC gains to the admissible feedforward bound, guaranteeing stability under saturation. This formulation is applicable to nonlinear, underactuated plants with hard constraints. To illustrate the methodology, the method is applied to a six-degree-of-freedom aircraft model and compared with Reinforcement Learning and isolated SMC. Simulation results show that the hybrid controller improves transient behavior and reduces control oscillations compared to standalone RL and SMC controllers, while preserving robustness under modeling uncertainties and disturbances. Even using it with partially trained policies, SMC component of the control stabilizes transients, whereas fully trained policies provide faster convergence, reduced constraint violations, and robustness. These results illustrate that learning-augmented control offers superior performance with robustness guarantees under tight input constraints.

**Index Terms** - nonlinear control, sliding mode control, reinforcement learning

## I. INTRODUCTION

Aircraft control across a broad flight envelope presents significant challenges due to the nonlinear nature of the underlying physics, high coupling between axes, and hard actuator constraints. As the vehicle transitions from low-angle, low-rate flight to high angles of attack or aggressive maneuvers, aerodynamic moments and forces become highly dependent on rate and attitude. In such conditions, control surface effectiveness varies with the state, and small control inputs can lead to large, coupled motions in

roll, pitch, and yaw. Additionally, phenomena like aerodynamic hysteresis or flow separation make the input–output relationship far from linear. Practical implementations of controllers also face constraints such as actuator rate limits, time delays, and saturation, all of which must be considered. During recovery maneuvers, the throttle is often fixed or manually adjusted, limiting the number of rapidly changing inputs and capturing engine dynamics, which leaves fewer independent control channels relative to the number of states.

In the past decade and a half, hybrid control architectures that integrate reinforcement learning (RL) with classical or modern feedback controllers have gained considerable attention across aerospace, robotics, and general nonlinear systems. Early works combined actor–critic RL with robust feedback laws such as RISE to achieve asymptotic tracking with theoretical stability guarantees in nonlinear systems [1]. Subsequent research explored RL augmentation of PID controllers, where the learning agent adjusts gains or generates feedforward commands to improve tracking and robustness without compromising stability [2], [3]. Similarly, RL has been combined with LQR to provide adaptive or residual control, leveraging LQR’s optimality and stability while allowing RL to compensate for model uncertainties or nonlinear effects [4], [5]. Model predictive control (MPC) has also been integrated with RL, either as a safety filter to enforce constraints or as a parameterized optimizer tuned by RL, enabling performance improvement while ensuring constraint satisfaction [5]. Sliding-mode control (SMC) has been paired with RL to combine robust finite-time convergence and disturbance rejection with learning-based adaptation for enhanced trajectory tracking [6]. More recently, feedforward–feedback architectures have emerged, in which RL learns anticipatory feedforward commands while a conventional feedback controller ensures stability and enforces constraints [7]. These hybrid approaches have been shown to performance, faster convergence, and enhanced robustness compared to standalone RL or feedback controllers, motivating the present study on RL–augmented hybrid control with safety filtering for nonlinear, constrained systems.

In this context, the goal of this paper is to design a controller for the post-stall spin recovery of a six-degree-of-freedom (6-DOF) F-18 model under conditions of input saturation, model uncertainty, and cross-axis coupling. While multiple control methods, such as sliding-mode control (SMC) and reinforcement learning (RL), can be used to address these challenges, each comes with its own set of trade-offs. This paper significantly extends our earlier work in [8] by introducing a bounded feedforward formulation for learning-based control, a tunable authority factor linking learned and robust control actions, and a Lyapunov-based stability analysis under actuator saturation.

Robust controllers like SMC are known for their stability guarantees but tend to be conservative, especially in highly nonlinear regimes. On the other hand, data-

driven controllers such as RL excel in handling complex dynamics but often lack formal safety guarantees and robustness in the presence of disturbances and uncertainties [9]. This motivates the integration of both methods into a hybrid controller that combines the strengths of an RL with the stability and robustness provided by SMC [10], [11].

The key contributions of this work are as follows:

- This work proposes a hybrid control methodology that combines Reinforcement Learning (RL) in the feedforward path with Sliding Mode Control (SMC) in feedback, ensuring both performance and robustness under hard actuator limits.
- A safety-filtered RL design is introduced, allowing the learning-based feedforward policy to operate within certified bounds while preserving the stability guarantees provided by the robust SMC feedback.
- The effectiveness of the hybrid controller is demonstrated in a challenging post-stall recovery scenario for a six-degree-of-freedom F-18 model, with comparisons drawn against standalone RL and SMC baselines.
- An implementation-ready framework is provided for integrating RL and SMC, enabling straightforward application to a wide range of platforms beyond the F-18 case study.

The remainder of this paper is organized as follows: Section II introduces the aircraft model and control task, defining the available state variables, control channels, and the constraints that must be considered during the control design. Section III discusses the RL framework used in the study, detailing the environment setup, observation and action spaces, reward shaping, and training configuration. Section IV presents the sliding-mode controller design, including methods for minimizing chattering and ensuring robustness against disturbances and model uncertainties. Section V explains how the hybrid RL-SMC controller is formulated, combining the feedforward RL component with the robust feedback from SMC under a simple coordination policy. Finally, Section VI presents results comparing the hybrid controller to RL-only and SMC-only controllers, demonstrating its performance improvements in terms of stability, convergence, and actuator usage.

## II. Model Description

This work considers a nonlinear model of the F-18/HARV, which exhibits many loss of control scenario via nonlinear phenomena. Aerodynamic data for this model is available for angle of attack range of -0.24 radians to 1.57 radians (-15° to 90°). Some key stability and control derivative data plots are shown in Fig. 1 and Fig. 2. Aerodynamic coefficients as function of state and control derivatives and state variables can be represented as:

$$\begin{aligned}
C_L &= C_{L_0} + C_{L_q} \frac{q \bar{c}}{2V} + C_{L_{\delta_e}} \delta_e, \\
C_D &= C_{D_0} + C_{D_q} \frac{q \bar{c}}{2V} + C_{D_{\delta_e}} \delta_e, \\
C_m &= C_{m_0} + C_{m_q} \frac{q \bar{c}}{2V} + C_{m_{\delta_e}} \delta_e, \\
C_Y &= C_{Y_\beta} \beta + C_{Y_p} \frac{p b}{2V} + C_{Y_r} \frac{r b}{2V} + C_{Y_{\delta_e}} \delta_e + C_{Y_{\delta_a}} \delta_a \\
&\quad + C_{Y_{\delta_r}} \delta_r, \\
C_l &= C_{l_\beta} \beta + C_{l_p} \frac{p b}{2V} + C_{l_r} \frac{r b}{2V} + C_{l_{\delta_e}} \delta_e + C_{l_{\delta_a}} \delta_a \\
&\quad + C_{l_{\delta_r}} \delta_r, \\
C_n &= C_{n_\beta} \beta + C_{n_p} \frac{p b}{2V} + C_{n_r} \frac{r b}{2V} + C_{n_{\delta_e}} \delta_e + C_{n_{\delta_a}} \delta_a \\
&\quad + C_{n_{\delta_r}} \delta_r.
\end{aligned}$$

The 6-DOF rigid body flight system governing equations based on [12] are given from (1) to (10).

$$\dot{V} = \frac{1}{m} \left[ T_m \eta \cos \alpha \cos \beta - \frac{1}{2} \rho V^2 S C_D(\alpha, q, \delta_e) - mg \sin \gamma \right] \quad (1)$$

$$\begin{aligned}
\dot{\alpha} &= q - \frac{1}{\cos \beta} [(p \cos \alpha + r \sin \alpha) \sin \beta] \\
&\quad + \frac{1}{mV} \left\{ T_m \eta \sin \alpha + \frac{1}{2} \rho V^2 S C_L(\alpha, q, \delta_e) - mg \cos \mu \cos \gamma \right\}
\end{aligned} \quad (2)$$

$$\begin{aligned}
\dot{\beta} &= \frac{1}{mV} \left[ -T_m \eta \cos \alpha \sin \beta + \frac{1}{2} \rho V^2 S C_Y(\alpha, \beta, p, r, \delta_e, \delta_a, \delta_r) \right] \\
&\quad + mg \sin \mu \cos \gamma + (p \sin \alpha - r \cos \alpha)
\end{aligned} \quad (3)$$

$$\dot{p} = \frac{I_y - I_z}{I_x} qr + \frac{1}{2I_x} \rho V^2 S b C_l(\alpha, \beta, p, r, \delta_e, \delta_a, \delta_r) \quad (4)$$

$$\dot{q} = \frac{I_z - I_x}{I_y} pr + \frac{1}{2I_y} \rho V^2 S c C_m(\alpha, q, \delta_e) \quad (5)$$

$$\dot{r} = \frac{I_x - I_y}{I_z} pq + \frac{1}{2I_z} \rho V^2 S b C_n(\alpha, \beta, p, r, \delta_e, \delta_a, \delta_r) \quad (6)$$

$$\begin{aligned}
\dot{\mu} &= \sec \beta (p \cos \alpha + r \sin \alpha) + \frac{1}{mV} \left\{ \frac{1}{2} \rho V^2 S C_L \tan \beta \right. \\
&\quad \left. + T_m \eta \sin \alpha + \sin \mu \tan \gamma - mg \cos \mu \cos \gamma \tan \beta \right. \\
&\quad \left. + \frac{1}{2} \rho V^2 S C_Y \cos \mu \tan \gamma \right\}
\end{aligned} \quad (7)$$

$$\begin{aligned}
\dot{\gamma} &= \frac{1}{mV} \left\{ T_m \eta (\sin \alpha \cos \mu + \cos \alpha \sin \beta \sin \mu) \right. \\
&\quad \left. - \frac{1}{2} \rho V^2 S C_L \cos \mu - mg \cos \gamma - \frac{1}{2} \rho V^2 S C_Y \sin \mu \right\}
\end{aligned} \quad (8)$$

$$\begin{aligned}
\dot{x} &= \frac{1}{mV \cos \gamma} \left\{ T_m \eta (\sin \alpha \sin \mu - \cos \alpha \sin \beta \cos \mu) \right. \\
&\quad \left. + \frac{1}{2} \rho V^2 S (C_L \sin \mu + C_Y \cos \mu) \right\}
\end{aligned} \quad (9)$$

The model can be represented in the nonlinear state-space form as:

$$\dot{x} = f(x) + g(x) \text{sat}(u) \quad (10)$$

Where  $x$  are the states and  $u$  are the control inputs of the aircraft model.

$$x(t) = [V, \alpha, \beta, p, q, r, \mu, \gamma]$$

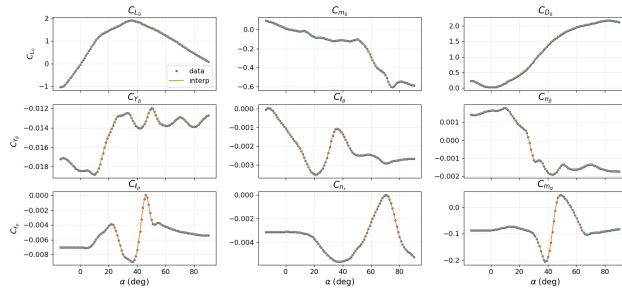


Fig. 1. Key coefficients and stability derivatives vs  $\alpha$ .

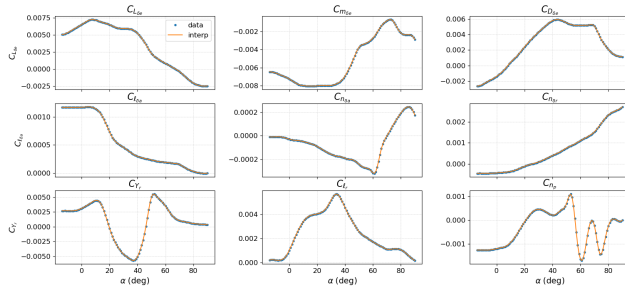


Fig. 2. Control coupling and dynamic derivatives vs  $\alpha$ .

$$u(t) = [\eta, \delta_e, \delta_a, \delta_r].$$

This is an underactuated system. Here, the  $\text{sat}(u)$  function models the constraints on the input term.

$$\text{sat}(u) = \begin{cases} u_{\max} & \text{if } u > u_{\max} \\ u & \text{if } u_{\min} \leq u \leq u_{\max} \\ u_{\min} & \text{if } u < u_{\min} \end{cases}$$

As the work presented in this paper is related to the faster dynamics, slower dynamics input  $\eta$  is kept fixed at a constant value. Only control inputs used are  $u \equiv [\delta_e, \delta_a, \delta_r]$ ,  $u \in \mathbf{R}^3$ .

### III. Control Methods

This section illustrates three control elements that complement each other and how they are combined. The first section explains reinforcement learning, an incremental decision-making method. It learns an interaction-based policy mapping states to commands. Proximal Policy Optimization helps make gradual, conservative changes that respect the rules. The second section explains sliding mode control as a robust feedback method. It describes the sliding objective, applying input-output linearization to focus on controlled areas, and how to reduce unwanted oscillations by using boundary layers or higher-order designs without sacrificing actuator movement and speed limits. The third section describes a combination where the learned policy is used initially to support fast response and coordination between axes. Fig. 3 shows the block

diagram of the architecture of the proposed controller. The trained policy tries to keep the system at safe limits while the sliding-mode law closes the loop to ensure precision and reliability despite uncertainty. All of these sections in aggregate represent a design plan: stabilize rates before achieving accurate position recovery, specify constraints clearly, and train using varied scenarios. They also show how all this is combined into a ready-to-fly system [13], [14].

#### A. Reinforcement Learning

Reinforcement learning (RL) deals with sequential decision-making problems where there are no labeled targets but only feedback in the form of reward-only. An agent continues to interact with an environment, from a given state it selects an action, the environment returns a new state and a reward, and learning is done by trial and error. Improvement is based on a trade-off between exploration (trying something else in order to get information) and exploitation (doing what appears to be working at the moment) so as to maximize long-term return.

When framed as a Markov Decision Process (MDP), good behavior is described in terms of Bellman optimality relations [15]. The behavior of the agent is captured by a policy  $\pi(a | s)$ , i.e., a control law that specifies a probability for every action in a state. Learning operates to refine this policy to an optimal policy,  $\pi^*(a | s)$ , that maximizes cumulative expected reward. Value functions are used to estimate states or state-action pairs under a policy, and there are various families of algorithms that use them in different manners. Value-based methods estimate them and act greedily, policy-based methods update policy parameters directly and the actor-critic and other hybrids do both. These approaches have been found beneficial in robotics, games, networked systems, and autonomous platforms [6], [7].

Proximal Policy Optimization (PPO) is an on-policy method which says the policy utilized to sample data is the one to be updated, eliminating the necessity of a replay buffer employed by off-policy methods such as DQN or DDPG. PPO follows a stochastic policy, samples new trajectories employing the current policy for each training iteration, and subsequently updates that policy based on the recently sampled on-policy batch. This is finalized to optimize the policy and maintain updates stable and conservative [16].

Proximal Policy Optimization (PPO) promotes exploration by adding an entropy term to its loss while keeping updates small enough for stable learning. It was designed as a practical alternative to Trust Region Policy Optimization (TRPO): instead of solving a heavy constrained problem each step, PPO uses simple surrogate objectives that approximate a trust region. Two variants are common, one penalizes deviations with a KL term, and the other “clips” the probability ratio. The clipped form is widely used because it curbs overly large policy

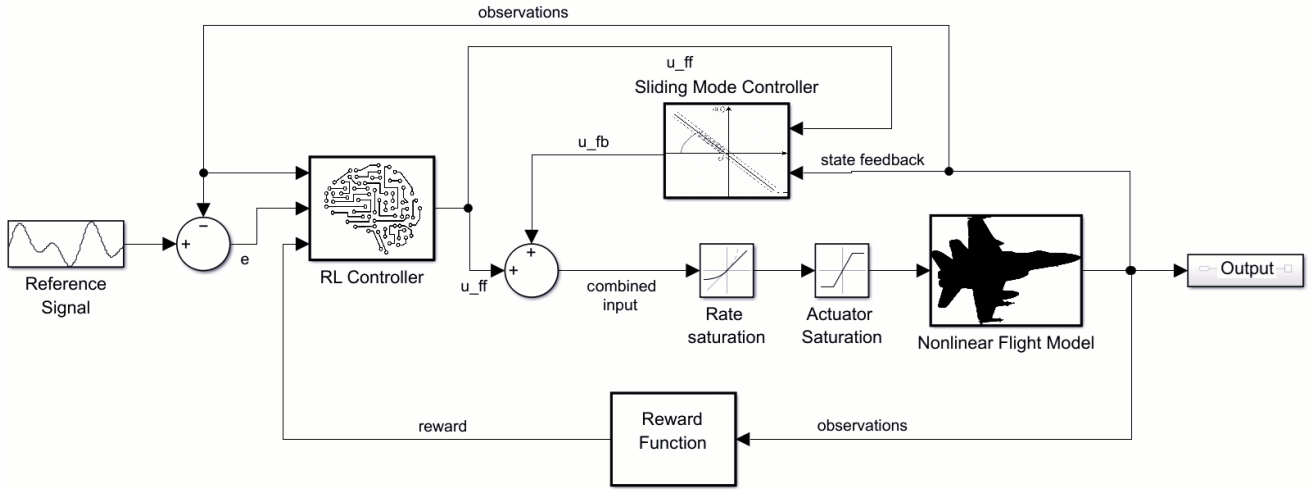


Fig. 3. A schematic block diagram of proposed controller using integration of the RL and SMC control.

shifts and keeps training steady. Introduced by Schulman and colleagues, PPO delivers reliable, sample-efficient policy improvements, addressing the instability that can arise when classic policy-gradient methods take steps that are too large [17].

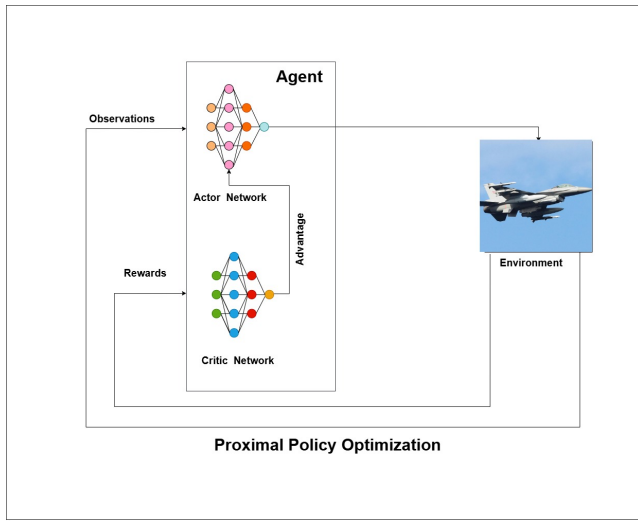


Fig. 4. Proximal Policy Optimization Structure for Flight Control.

This work casts the control problem as a Markov Decision Process described by  $(s, a, p, r, \Gamma)$ : the state, action, transition probability, reward, and a discount factor that balances near-term and long-term returns. PPO constrains how far the new policy may move from the old one within this MDP setting by operating on an on-policy batch and restricting the effective step size. In this work, a reinforcement learning (RL) environment for the aircraft model is developed and trained using Proximal Policy Optimization (PPO), owing to its demonstrated effectiveness in control

applications. The architecture of the agent–environment interaction is illustrated schematically in Fig. 4.

PPO uses a objective function that penalizes the updates of the policy if it updates the policy beyond a threshold value. The objective function is defined by :

$$r_t(\theta) = \frac{\pi_\theta(a_t | s_t)}{\pi_{\theta_{\text{old}}}(a_t | s_t)} \quad (11)$$

$$L^{\text{clipped}} = E[\min(R(\theta).A_t, \text{clip}(R(\theta), 1 - \epsilon, 1 + \epsilon)A_t)]. \quad (12)$$

Here  $E$  is Expectation,  $\epsilon$  is the clipping range,  $A_t$  represents the advantage value.

The algorithm of PPO can be described as:

---

**Algorithm 1 PPO algorithm**

---

```

1: Initialize the actor network  $\pi_\theta$  and the value network  $V_\phi$ 
2: for Iteration = 1, 2, ..., M do
3:   for Episode = 1, 2, ..., N do
4:     for  $t = 1, 2, \dots, T$  do
5:       Using policy  $\pi_\theta$  choose an action  $a_t$ 
6:       If termination conditions hold true, end the episode
7:     end for
8:     Find advantage values  $A_1, A_2, \dots, A_T$  using  $V_\phi$ 
9:   end for
10:  for Epochs = 1, 2, ..., K do
11:    Update actor network using value  $L^{\text{CLIP}}$ 
12:    Update value using critic loss
13:  end for
14: end for

```

---

## B. Sliding Mode Control

Because of their intrinsic non-linearity and discontinuity, Sliding Mode Controllers (SMC) are particularly

well-suited for the control of intricate non-linear systems such as aerial vehicles. In SMC, the approach includes the specification of a sliding surface, and an appropriate switching logic is formulated to keep the system trajectories on the surface. When the trajectories stray from the surface, they are pushed back onto the sliding surface. This corrective action, however, causes small-amplitude, high-frequency oscillations in the system inputs, an effect known as chattering [1][2]. Many techniques can be used to reduce this chattering, such as higher-order sliding mode control [3][4], boundary layer techniques, and the power rate reaching law [18], [19].

Sustaining a leveled flight state requires state controls  $\alpha$ ,  $\beta$ , and  $\mu$ . These are the angle of attack ( $\alpha$ ) of the aircraft, angle of sideslip ( $\beta$ ), and wind-axis roll angle ( $\mu$ ). Each variable is assigned to stability in one axis:  $\alpha$  for pitch,  $\beta$  for yaw, and  $\mu$  for roll. The controller omits the control surface aerodynamic force terms compared to control moments because their influence is negligible [20]. This simplification also removes non-minimum phase behavior from the controller dynamics, which facilitates an easier control law design [21], [22]. Under this assumption, it can be seen from the (1) to (9) that for each output variable, a control input term appears only after the output variable is differentiated twice with respect to time. This sets the relative degree ( $\varsigma$ ) of each of the output variables to 2. The relative degree of a state is the number of its time derivatives needed before the input can be seen within the resulting expression. The aggregate relative degree for this system is 6, which is less than the overall system order [23]. Here, the system order is 8 and ( $\varsigma_{sys} = 6 < 8$ ) minus the combined relative degree represents the internal dynamics of the system. These are shaped by the throttle input, which is maintained at a steady value [12]. With the help feedback linearization, one can convert the coupled system of order 6 to 3 decoupled systems of order 2 which can be seen in (22). This helps in dealing the system equations with variables as scalars instead of matrices.

For a second order system ( $\varsigma = 2$ ),

$$\dot{x}_1 = x_2 \quad (13)$$

$$\dot{x}_2 = f(x) + g(x)u \quad (14)$$

$$y = h(x) \quad (15)$$

Let  $e = y - y_{ref}$  be the tracking error. Therefore,

$$\dot{e} = \dot{y} - \dot{y}_{ref} \quad (16)$$

$$\ddot{e} = \ddot{y} - \ddot{y}_{ref} \quad (17)$$

Constructing the sliding surface  $\emptyset$  as:

$$\emptyset = \dot{e} + \lambda_1 e + \lambda_2 \int_0^t e d\tau. \quad (18)$$

Designing control  $u$  as:

$$u = g(x)^{-1}(u_r + u_s) \quad (19)$$

$$u_r = -f(x) + \ddot{y}_{ref} - \lambda_1 \dot{e} + \lambda_2 e \quad (20)$$

$$u_s = -(K|s|^{1/2} + \epsilon) sign(\emptyset). \quad (21)$$

The output variables are  $y = [\alpha, \beta, \mu]$ . Since, there are couplings in longitudinal and lateral-directional dynamics of the aircraft, this work uses the input-output linearization to transform the system inputs [21], [23].

Consider  $z_1 = y = [\alpha, \beta, \mu]$ .

$$z_2 = \dot{y} = \begin{bmatrix} L_f \alpha \\ L_f \beta \\ L_f \mu \end{bmatrix}$$

$$\dot{z}_2 = \ddot{y} = \begin{bmatrix} L_f^2 \alpha \\ L_f^2 \beta \\ L_f^2 \mu \end{bmatrix} + \begin{bmatrix} L_g L_f \alpha \\ L_g L_f \beta \\ L_g L_f \mu \end{bmatrix} u = \nu \quad (22)$$

Here  $\nu$  is the auxiliary input and  $L_f y$  represents Lie derivative of  $y$  along the vector field  $f(x)$ .

$$L_f y = \frac{\partial y}{\partial x} f(x) = \nabla y^T f(x) \quad (23)$$

Finally, the control input can be calculated from auxiliary input [23] as:

$$u = L_g L_f y^{-1}(\nu - L_f^2 y).$$

### C. RL-SMC based Hybrid control

In this work, hybrid control design that pairs a reinforcement-learning feedforward module with a sliding-mode feedback law was developed. The reinforcement-learning policy is trained in simulation across a wide range of starting states, aerodynamic parameters, sensor noise, delays, and gusts. After training, it runs onboard as a fast state-to-command mapping that proposes anticipatory, coordinated surface deflections. In practice, it learns the kinds of “look-ahead” moves that shorten transients, reduce overshoot, and take advantage of natural couplings between roll, pitch, and yaw. Fig. 3 shows the proposed architecture’s block diagram.

Because a learned policy does not come with formal guarantees and can misgeneralize outside its training envelope, its contribution is deliberately limited and checked before it reaches the actuators. It is important to place a hard bound on how much authority the learned policy may exercise and pass its suggestion through a safety filter. This filter enforces deflection and rate limits, honors actuator dynamics, and ensures the baseline stability

condition is not compromised. If the learned suggestion would violate these rules, the filter minimally modifies it; if necessary, it blocks it entirely.

The backbone of the system is the sliding-mode controller. It is responsible for meeting the tracking goal and for robustness against modeling errors and disturbances that act through the same channels as the control surfaces. The sliding-mode law combines a steady “equivalent” component that cancels the known part of the dynamics with a high-gain corrective component that guarantees fast convergence into a small neighborhood of the target. Its gains are selected to dominate the worst-case combination of plant disturbance and the maximum contribution allowed from the learned policy. In effect, the filtered learned input appears to the sliding-mode analysis as a bounded, matched perturbation that has already been accounted for.

Training of the learned policy reflects these design choices. Rewards emphasize quick damping of body-rate excursions, prompt but well-behaved attitude recovery, low control activity changes from one instant to the next, and strict compliance with deflection and rate limits. Domain randomization ensures the policy sees many plausible aircraft conditions rather than a single “perfect” model. At deployment, the allowed authority for the learned policy can be scheduled with flight condition: higher in well-modeled regions, lower near stall, saturation, or other edges of the envelope.

This arrangement preserves the strengths of both components. The sliding-mode controller provides the certificate of stability and robustness; the learned policy improves performance within clearly defined, enforced limits. A supervisory layer monitors out-of-distribution states and repeated safety interventions; when these are detected, the system falls back to sliding-mode-only operation until conditions return to normal. The result is a controller that keeps the guarantees expected in flight-critical applications while harvesting the performance gains that modern learning methods can offer.

#### IV. Implementation

As discussed in section II, first an RL based environment for the aircraft model is created using OpenAI gym. The Observation space and action space of the gym environment is defined as follows:

##### A. Training of the RL Model

To effectively control the aircraft and to bring it to a steady flight condition, the angular rates ( $p$ ,  $q$  and  $r$ ) of aircraft should be brought down to lower values; after this to maintain a leveled flight condition, the control of states  $\alpha$ ,  $\beta$ , and  $\mu$  is required which helps in attitude stabilization. From (1) and (9), it can be seen that as long as  $\alpha$ ,  $\beta$ ,  $\mu$  and angular rates are stabilized,  $V$  and  $\gamma$  will also be stabilized to finite value, subjected to condition that  $\eta$  does not change.

TABLE I  
Observation and Action Space for F-18 RL Environment (All Angles in Radians)

Type	Variable (Unit)	Dim.	Range	Ref.
Obs.	Airspeed $V$ (ft/sec)	1	[0, 2000]	—
	AoA $\alpha$ (rad)	1	[-0.244, 1.571]	$\alpha_{ref}$
	Sideslip $\beta$ (rad)	1	[- $\pi$ , $\pi$ ]	$\beta_{ref}$
	Bank angle $\mu$ (rad)	1	[- $\pi$ , $\pi$ ]	$\mu_{ref}$
	Angular rates $p, q, r$ (rad/s)	3	[-10 $\pi$ , 10 $\pi$ ]	0
	Flight path angle $\gamma$ (rad)	1	[-1.745, 1.745]	—
Act.	Elevator $\delta_e$ (rad)	1	[-0.436, 0.175]	—
	Aileron $\delta_a$ (rad)	1	[-0.436, 0.436]	—
	Rudder $\delta_r$ (rad)	1	[-0.524, 0.524]	—

The first priority should be attenuation of the angular rates and then create a leveled flight attitude condition. Therefore, the design of the reward function should be carefully done so that it emphasizes more on controlling the angular rates initially, and once the angular rates drop below a threshold value, then the reward function should prioritize maintaining the leveled flight at target angles [24]. Designing a continuous reward structure for the RL environment is done in two phases. In the first phase, agent only focuses on rates and in the second phase, agent prioritizes attitude angles in addition to angular rates. To accelerate the training, the Potential Based Reward Shaping (PBRs) is also used [25].

The reward structure is defined as:

*Phase 1*

When  $|p, q, r| > 0.17 \text{ rad/sec}$

$$r_{phase1} = -\|\omega\|^2 - w_{p1}(|pq| + |qr| + |pr|). \quad (24)$$

Where:

$$\|\omega\| = \sqrt{p^2 + q^2 + r^2}.$$

$|pq| + |qr| + |pr|$  term represents the couplings between the three axes, which is also undesirable, so it is penalized as well.  $w_{p1}$  is the weight factor for scaling the weights of the rate penalty and cross-coupling penalty.

*Phase 2*

When  $\|\omega\| < 0.17 \text{ rad/sec}$

$$r_{phase2} = -e_\alpha^2 - w_{p21}e_\alpha q - w_{p22}(\|\omega\|^2 + |pq| + |qr| + |pr|) \quad (25)$$

Additional Reward:

$$\begin{aligned} &+5 \text{ if } |e_\alpha| < 0.017 \text{ rad} \\ &+3 \text{ if } |e_\beta| < 0.017 \text{ rad} \\ &+3 \text{ if } |e_\mu| < 0.017 \text{ rad} \\ &- \sum_i action_i^2. \end{aligned}$$

Where:

$$\begin{aligned} e_\alpha &= \alpha - \alpha_d \\ e_\beta &= \beta - \beta_d \\ e_\mu &= \mu - \mu_d. \end{aligned}$$

A sudden jump in reward change from phase 1 to phase 2 may affect the training so a logistic gate blend function  $\varepsilon(\|\omega\|)$  is added to make a smooth shift from phase 1 to phase 2.

Let

$$\varepsilon(\|\omega\|) = \frac{1}{1 + \exp(k_{\text{blend}}(\|\omega\| - \omega_{\text{th}}))}, \quad (26)$$

with  $k_{\text{blend}} = 10$  and  $\omega_{\text{th}} = 0.17 \text{ rad/s}$ . The raw performance reward is

$$r_{\text{raw}} = (1 - \varepsilon)r_{\text{phase1}} + \varepsilon r_{\text{phase2}}. \quad (27)$$

When rates are high,  $\varepsilon \approx 0$  and Phase 1 dominates; when rates are small,  $\varepsilon \approx 1$  and Phase 2 dominates.

The variables  $\alpha_d$ ,  $\beta_d$ , and  $\mu_d$  denote the target values for the angle of attack, sideslip angle, and bank angle, respectively. To simplify the design of the reward structure, continuous rewards are not explicitly assigned for deviations in sideslip angle  $\beta$  and bank angle  $\mu$ . This is justified by the inherent symmetry of the aircraft, which suggests that these states will naturally tend toward zero over time. Instead, the stabilization of roll and yaw rates  $p$  and  $r$  is expected to indirectly contribute to restoring  $\beta$  and  $\mu$  to their nominal values. In the second reward phase, the weighting coefficient  $w_{p_{22}}$  should be chosen carefully—large enough to ensure correction of coupling errors and rate stabilization, but not so large that it overwhelms the other objectives.

Traditional continuous penalty-based rewards apply a constant cost at each step, regardless of whether the agent is progressing toward or away from the goal. In contrast, Potential-Based Reward Shaping (PBR) introduces direction-sensitive feedback, assigning positive values when the agent moves closer to the desired state and negative values when it deviates [25]. Although PBR does not alter the set of optimal solutions, it significantly improves training efficiency by offering a more informative gradient to guide policy learning.

$$\sigma = -e_\alpha^2 - w_{p_{21}} \|\omega\|^2 \quad (28)$$

Here  $\sigma$  is the reward shaping potential. From (27) and (28), the total reward achieved is:

$$\text{Reward} = r_{\text{raw}} + \Gamma \sigma_{t+1} - \sigma_t. \quad (29)$$

The term  $\sigma_t$  represents the potential function evaluated at the current timestep, while  $\sigma_{t+1}$  corresponds to the potential at the subsequent step, based on the predicted trajectory. The discount factor  $\Gamma$  is a critical hyperparameter in PPO training, controlling how much the agent values long-term rewards relative to immediate ones. This same discount factor is also employed in shaping the PBR-based reward, ensuring consistency between policy optimization and reward guidance.

For training and evaluation, the nonlinear dynamics of the F-18/HARV aircraft model were implemented within a custom environment based on the OpenAI Gym interface [26]. This tailored Gym environment was designed to accurately capture the system's state representation, permissible action set, and underlying equations of motion. Specific terminal conditions were introduced to detect situations where the aircraft exceeds its operational flight envelope or significantly diverges from the desired target states. A large negative reward of  $-1000$  was assigned when such terminal conditions were triggered. This value is decided relative to maximum possible cumulative reward. The structure and control flow governing the environment's simulation logic are described in Algorithm 2. Detailed bounds for the observation and action spaces are provided in Table I.

---

**Algorithm 2 F-18 Environment Logic 6 DOF**

---

```

1: Input: Initial state  $x_0$ , timestep  $\Delta t$ , control  $a_t$ 
2: Initialize F-18 state vector and aircraft parameters
3: function reset ()
4:   Sample target angle of attack  $\alpha \in [-5^\circ, 40^\circ]$ 
5:   Initialize state  $x_0 = [V, \alpha, \beta, p, q, r, \dots]$ 
6:   return initial observation  $s_0$ 
7: end function
8: function step( $a_t$ )
9:   Clip and scale  $a_t$  to control limits
10:  Compute control input  $u_t$  using Env actions  $a_t$ 
11:  Integrate aircraft dynamics:  $x_{t+1} = f(x_t, u_t)$ 
12:  Update positions and Euler angles
13:  Compute reward: Potential-based reward shaping or error-based penalty
14:  Check termination conditions
15:  return  $(s_{t+1}, r_t, d_t, \text{info})$ 
16: end function

```

---

The observation vector consists of the following states:

$$s = \{V, \alpha, \beta, p, q, r, \mu, \gamma, \alpha_d, \beta_d, \mu_d\} \quad (30)$$

Action space is defined as:

$$a = \{\delta_e, \delta_a, \delta_r\} \quad (31)$$

Simulation is randomly initialized at the random state in the flight envelope at each episode. The bounds of the random states for episode initialization are shown in Table II. At the start of simulation the altitude of aircraft is assumed at 0 ft. so that loss of altitude can be analyzed with ease.

The weights  $w_{p_1}$ ,  $w_{p_{21}}$  and  $w_{p_{22}}$  were kept 0.3, 0.3 and 0.05 respectively. Target value  $\alpha_d$  is also randomized for every episode between  $-0.085$  radians to  $0.68$  radians.  $\beta_d$  and  $\mu_d$  are kept to zero. The control inputs are subject to predefined saturation limits to simulate real-world actuator constraints. The actuator constraints for elevator, aileron and rudder are  $(-25^\circ, 10^\circ)$ ,  $(-25^\circ, 25^\circ)$  and  $(-30^\circ, 30^\circ)$  respectively. The control objective is to

TABLE II

Bounds for random initialization of state (Angles in Radians; Speed in ft/sec)

State Variable (Unit)	Lower Bound	Upper Bound
Airspeed $V$ (ft/sec)	100	1500
Angle of Attack $\alpha$ (rad)	-0.175	1.047
Sideslip Angle $\beta$ (rad)	-0.262	0.262
Roll Rate $p$ (rad/s)	-2.094	2.094
Pitch Rate $q$ (rad/s)	-1.047	1.047
Yaw Rate $r$ (rad/s)	-0.524	0.524
Bank Angle $\mu$ (rad)	-3.142	3.142
Flight Path Angle $\gamma$ (rad)	-1.047	1.047
Desired AoA $\alpha_d$ (rad)	-0.085	0.68
Desired Sideslip $\beta_d$ (rad)	0	0
Desired Bank Angle $\mu_d$ (rad)	0	0

track reference trajectories for key state variables (e.g.,  $\alpha$ ,  $p$ ,  $q$ ,  $r$  etc.) while ensuring that the system can converge to the desired values. Training of the RL agent was carried out using Stable-Baselines3(SB3) which is a popular Python-based open-source library for reinforcement learning algorithms [27]. Proximal Policy Optimization Algorithm was used as it is sample efficient and robust in the training process. The network architecture is an Actor-Critic Network of (256, 128) hidden layers - Tanh configuration each. This size was decided empirically after running multiple simulations with different network sizes to avoid overfitting. Learning rate and Discount factor were kept at 5e-5 and 0.99 to encourage smooth learning and long-term rewards. The agent was trained for a total of 6000 episodes. Each episode consists of 20000 timesteps, with one timestep being of size 0.01 seconds. Agent training performance was logged to check the reward trend with ongoing training using Tensorboard. The trained model will give the output  $u_{RL}$  which will be used as the feedforward control input  $u_{ff}$ .

### B. Integration of Feedforward and Feedback control architectures

For integrating the feedforward term in the SMC feedback controller, some modifications to the system formulation are required.

$$\dot{x}_1 = x_2 \quad (32)$$

$$\dot{x}_2 = f(x) + g(x)u + d(x, t) \quad (33)$$

The scalar  $\zeta \in (0, 1]$  is introduced as a control authority factor that modulates the contribution of the sliding mode feedback term. Specifically,  $\zeta$  determines the relative dominance of the feedback controller with respect to the feedforward (RL-based) policy.

Now, the control input is a combination of feedforward and feedback terms:

$$u = u_{ff} + u_{fb} = u_{RL} + \zeta u_{SMC} \quad (34)$$

Without the introduction of the scaling factor  $\zeta$ , the high-gain and discontinuous nature of the sliding mode controller can dominate the composite control input,

thereby suppressing the behavior learned by the reinforcement learning policy. The parameter  $\zeta$  therefore enables a structured blending of learning-based feedforward control with model-based robust feedback, preserving the performance advantages of the RL control while ensuring stability and disturbance rejection through SMC.

For ideal feedforward control using only  $u = u_{ff}$ :

$$\dot{x}_2 = f(x) + g(x)u_{ff} \quad (35)$$

However, if  $u_{ff}$  is insufficient for perfect tracking:

$$\dot{\hat{x}}_2 = f(x) + g(x)u_{ff} \neq \dot{x}_2 \quad (36)$$

The resulting mismatch term is:

$$\delta(x) = \dot{\hat{x}}_2 - \dot{x}_2 \quad (37)$$

Substituting (34) into the original system dynamics:

$$\dot{x}_2 = f(x) + g(x)(u_{ff} + u_{fb})$$

$$\dot{x}_2 = \dot{\hat{x}}_2 + g(x)u_{fb} \quad (38)$$

(38) defines a new control system for the feedback controller to handle. Therefore, a sliding mode controller (SMC) is designed for the feedback input  $u_{fb}$ .

Define the tracking error as  $e = x_1 - y_{ref}$ , and the sliding surface as:

$$\varnothing = \dot{e} + \lambda_1 e + \lambda_2 \int_0^t e(\tau) d\tau \quad (39)$$

Then, the feedback control input is:

$$u_{fb} = g(x)^{-1} (u_r + u_s) \quad (40)$$

where

$$u_r = -\dot{\hat{x}}_2 + \ddot{y}_{ref} - \lambda_1 \dot{e} - \lambda_2 e \quad (41)$$

$$u_s = -K|\varnothing|^{1/2} \text{sign}(\varnothing) \quad (42)$$

Finally, after substituting from (41) and (42) the total control input becomes:

$$u = u_{ff} + g(x)^{-1} (-\dot{\hat{x}}_2 + \ddot{y}_{ref} - \lambda_1 \dot{e} - \lambda_2 e - K|\varnothing|^{1/2} \text{sign}(\varnothing)) \quad (43)$$

### V. Stability Analysis

Define the feedforward error as:

$$\delta(x) = \dot{\hat{x}}_2 - \dot{x}_2 \quad (44)$$

This measures how far the RL-predicted acceleration  $\hat{x}$  is from the true (ideal) model-based acceleration:

$$\dot{\hat{x}}_2 = f(x) + g(x)u_{ff}^{\text{ideal}} + d(x, t) \quad (45)$$

The sliding surface is defined as:

$$\varnothing = \dot{e} + \lambda_1 e + \lambda_2 \int_0^t e(\tau) d\tau \quad (46)$$

$$u = u_{ff} + u_{fb} \quad (47)$$

Differentiating (46):

$$\dot{\phi} = f(x) + g(x)u_{\text{ff}} + g(x)u_{\text{fb}} - \ddot{y}_{\text{ref}} + \lambda_1 \dot{e} + \lambda_2 e + d(x, t)$$

Substitute from (34):

$$\dot{\phi} = \dot{\bar{x}}_2 - \ddot{y}_{\text{ref}} + \lambda_1 \dot{e} + \lambda_2 e + g(x)\zeta u_{\text{SMC}}. \quad (48)$$

Then:

$$\dot{\phi} = -\zeta \kappa \cdot \text{sign}(\phi) + \delta(x) + d(x, t). \quad (49)$$

Where

$$\kappa = K|\phi|^{1/2} + \epsilon. \quad (50)$$

$\epsilon$  is small positive value that works as a gain when  $\phi \rightarrow 0$ . The ideal sliding condition is:

$$\dot{\phi} = -\zeta \kappa \cdot \text{sign}(\phi). \quad (51)$$

But due to imperfect feedforward:

$$\dot{\phi} = -\zeta \kappa \cdot \text{sign}(\phi) + \delta(x) + d(x, t). \quad (52)$$

So the term  $\delta(x) + d(x, t)$  acts like a disturbance or uncertainty.

Sliding dynamics:

$$\dot{\phi} = -\zeta \kappa \cdot \text{sign}(\phi) + \delta(x) + d(x, t). \quad (53)$$

### Stability Condition

Using Lyapunov Stability Criteria Lyapunov function candidate  $V_L$  as follows:

$$V_L = \frac{1}{2}\phi^2 \quad (54)$$

$$\dot{V}_L = \phi \dot{\phi}. \quad (55)$$

To ensure convergence, it requires:

$$\zeta \kappa > |\delta(x)| + |d(x, t)|. \quad (56)$$

Assume that the feedforward mismatch  $\delta(x)$  and the external disturbance  $d(x, t)$  are bounded such that

$$|\delta(x)| \leq \bar{\delta}, \quad |d(x, t)| \leq \bar{d}, \quad (57)$$

where  $\bar{\delta} > 0$  and  $\bar{d} > 0$  are known positive constants representing the worst-case bounds on the model uncertainty and disturbance, respectively.

In practice, due to the presence of bounded feedforward mismatch  $\delta(x)$  and disturbance  $d(x, t)$ , exact convergence to  $\phi = 0$  cannot be guaranteed. Instead, the system reaches in finite time a neighborhood  $\varrho$  of the sliding surface defined by (58)

$$|\phi| \leq \varrho \triangleq \frac{\bar{\delta} + \bar{d}}{\zeta \kappa}, \quad (58)$$

and remains bounded within this region thereafter.

(56) guarantees that the sliding variable reaches a bounded neighborhood of zero in finite time, even under feedforward model error  $\delta(x)$  [28], [29]. This also directly tells us that size of corrective sliding gain depends on the mismatch term  $\delta(x)$  directly. If one ignores the external disturbance term  $d(x, t)$  for simplicity, then if the RL model is perfectly trained such that  $\delta(x) \rightarrow 0$ , the boundary layer shrinks to the origin, which means control actions are fully generated by RL agent.

## VI. Simulation Results and Discussions

To justify the reward function that we have used in training the environment, the phase-plane plots of the control variables in the standalone RL simulation are plotted to demonstrate motivation behind the two phase reward structure. After that, to evaluate the proposed architecture, this work considers two experimental phases. In the first phase, it analyzes the effect of introducing the SMC safety layer into a partially trained RL policy. In the second phase, full comparative study of *RL-only*, *SMC-only*, and *RL-SMC hybrid* controllers using a fully trained RL policy tuned for spin recovery is conducted.

### A. Phase-Plane Analysis and Motivation for Reward Design

The phase-plane trajectories of  $(\alpha, \dot{\alpha})$ ,  $(\beta, \dot{\beta})$  and  $(\mu, \dot{\mu})$  reveal that the aircraft dynamics under spin recovery exhibit a limit-cycle-like behavior, particularly in the high-rate regime. The blue circle marks the beginning of the trajectory and black square marks its end. As shown in Fig. 5, a significant portion of  $\alpha$  trajectory lies in the region where the body-rate magnitude satisfies  $||\omega|| > 0.17$  rad/s (red trajectories). Similar trend can be seen in Fig. 6 and Fig. 7 for  $\beta$  and  $\mu$  variables. In this region, the states circulate along closed or slowly contracting orbits with strong cross-axis coupling, indicating that the dynamics are dominated by rotational energy rather than attitude error. This observation implies that direct penalization of attitude deviations in this regime is not effective and can interfere with rate dissipation if we try to incorporate it in our reward function in Phase 1.

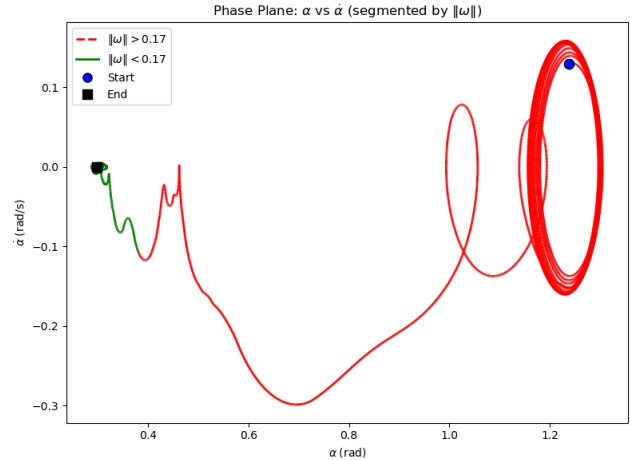


Fig. 5. Phase plane plot of angle of attack ( $\alpha$ ).

Once the body-rate magnitude drops below the threshold  $||\omega|| > 0.17$  rad/s (green trajectory), the limit-cycle behavior collapses and the trajectories contract toward the equilibrium. In this low-rate regime, the system transitions to near-equilibrium dynamics where attitude regulation becomes meaningful and well-conditioned. This clear

separation of dynamical regimes motivates the adopted two-phase reward structure where rate-dominant penalties are enforced while the system resides on the high-rate limit-cycle, and attitude-error penalties are introduced only after the trajectory exits this region. The smooth blending between these objectives ensures a consistent learning signal while respecting the underlying nonlinear dynamics of spin recovery.

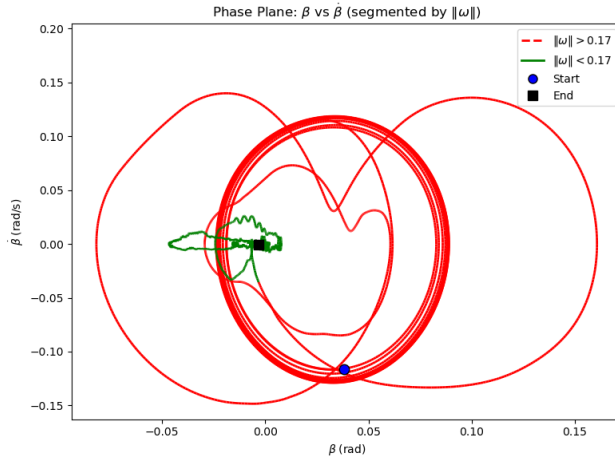


Fig. 6. Phase plane plot of angle of sideslip ( $\beta$ ).

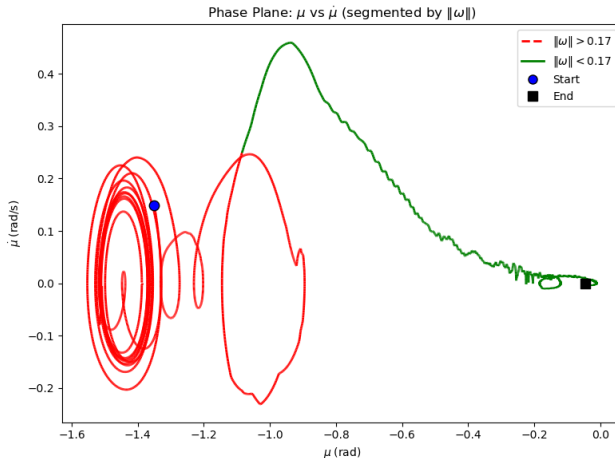


Fig. 7. Phase plane plot of bank angle ( $\mu$ ).

## B. Partially Trained RL Model: Effect of SMC Safety Layer

A Proximal Policy Optimization (PPO) agent was trained in the F-18/HARV upset-recovery environment for 10 million timesteps. The policy is not trained to achieve single target from a fixed initial condition but it was trained to track a range of target angle of attack  $\alpha$  in the range 0 to 0.698 radians ( $0^\circ$  to  $40^\circ$ ) from any random initial condition, therefore it retains noticeable

variability and occasional destabilizing actions in unseen and unexplored states.

To assess the safety-layer effect:

- **RL (partial trained PPO):** direct policy output applied to the plant, subject only to actuator saturation limits [30], [31].
- **RL with SMC feedback:** the same partial policy filtered through the proposed SMC feedback loop, which overrides the RL output whenever stability is at risk.

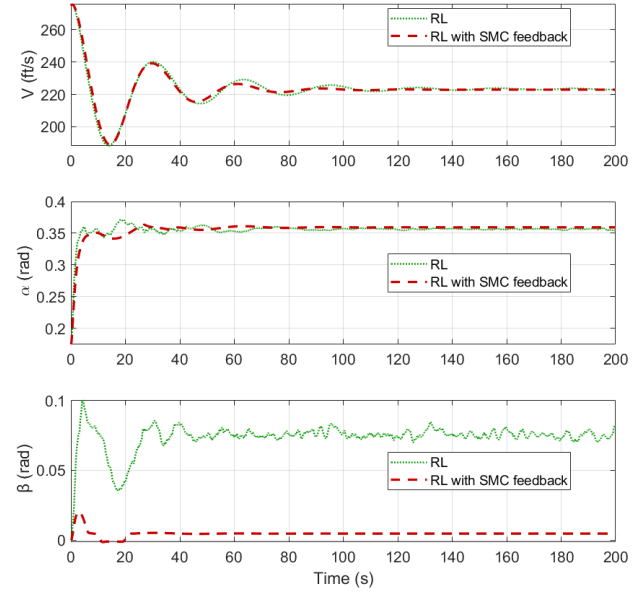


Fig. 8. System response for a partially trained PPO policy when target angle of attack is  $0.349$  rad ( $20^\circ$ ):  
(a) velocity ( $V$ ) (ft/sec) (b) angle of attack ( $\alpha$ ) (rad) (c) angle of sideslip ( $\beta$ ) (rad).

Figs. 8 - 11 (time histories of states and control-surface deflections) show that in RL-only simulation, the aircraft exhibits oscillatory trajectories, with  $\alpha$  overshoots in Fig. 8(b), small but significant offset error in angle of sideslip in Fig. 8(c), yaw rates persisting for a long time period in Fig. 9(c). In RL simulation with SMC feedback case, the overshoot is comparatively reduced, the rates settle to zero, and control usage remains smooth, despite the underlying policy being only partially converged. The control inputs in the RL-only case exhibit significant chattering, whereas the addition of SMC feedback substantially suppresses these high-frequency oscillations, making them practically negligible as seen in Fig. 11.

The same partially trained model is used in the simulation for tracking a different target angle of attack, i.e.,  $0.52$  rad ( $30^\circ$ ), in order to evaluate the generalization capability of the learned policy beyond the training condition.

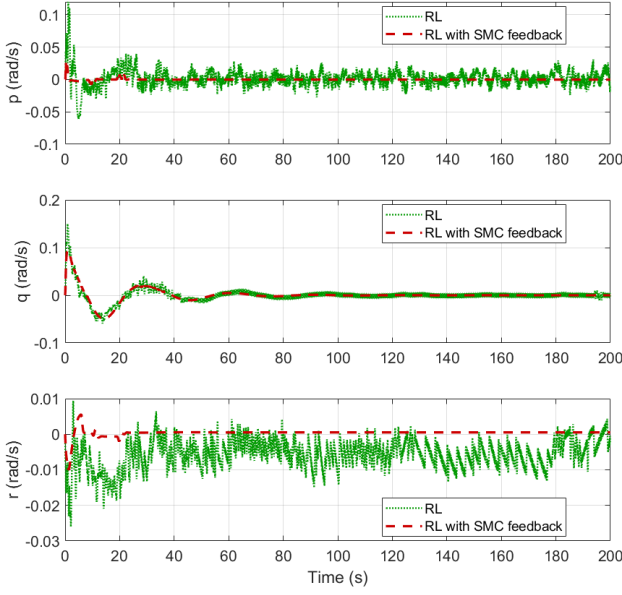


Fig. 9. System response for a partially trained PPO policy when target angle of attack of  $0.349 \text{ rad}$  ( $20^\circ$ )  
 (a) roll rate ( $p$ ) ( $\text{rad/sec}$ ) (b) pitch rate ( $q$ ) ( $\text{rad/sec}$ ) (c) yaw rate ( $r$ ) ( $\text{rad/sec}$ ).

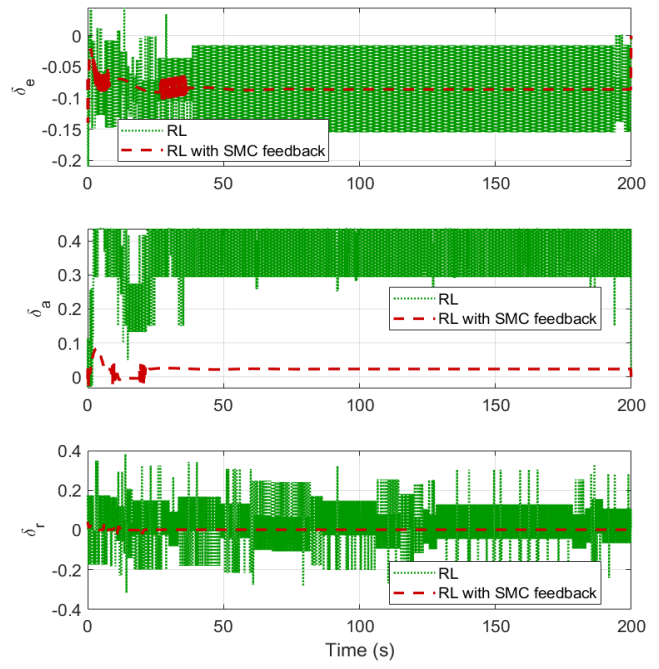


Fig. 11. Control surface deflection values generated by partially trained PPO policy when target angle of attack of  $0.349 \text{ rad}$  ( $20^\circ$ )  
 (a) elevator ( $\delta_e$ ) ( $\text{rad}$ ) (b) aileron ( $\delta_a$ ) ( $\text{rad}$ ) (c) rudder ( $\delta_r$ ) ( $\text{rad}$ ).

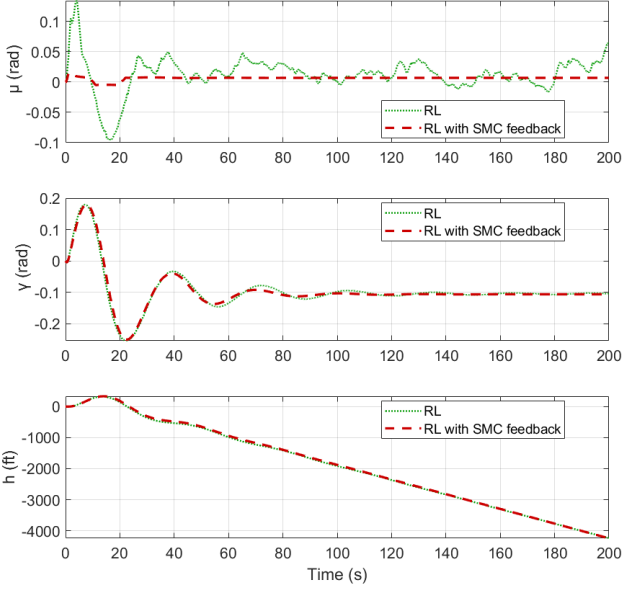


Fig. 10. System response for a partially trained PPO policy when target angle of attack of  $0.349 \text{ rad}$  ( $20^\circ$ )  
 (a) bank angle ( $\beta$ ) ( $\text{rad}$ ) (b) flight path angle ( $\gamma$ ) ( $\text{rad}$ ) (c) altitude ( $h$ ) ( $\text{ft}$ ).

Similar results can be seen in Figs. 12 - 15, where in Fig. 16(b) angle of attack in RL only simulation shows overshoot compared to the simulation of RL with SMC feedback.

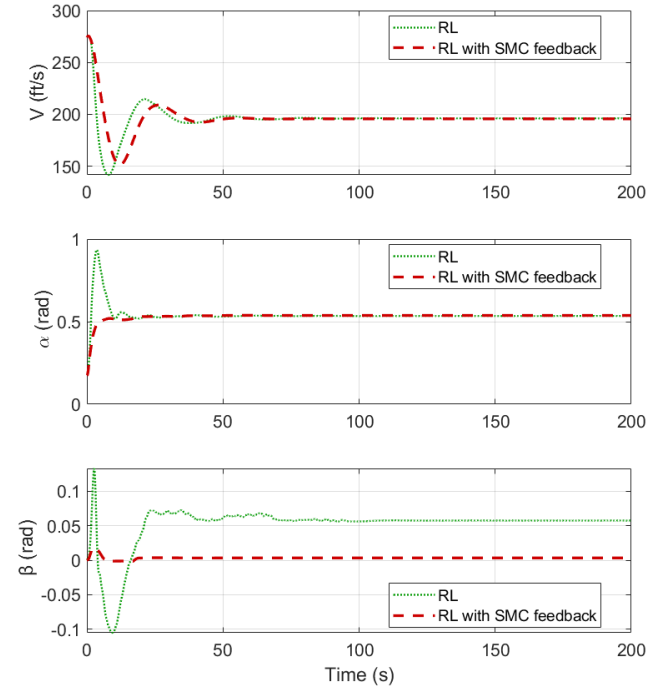


Fig. 12. System response for a partially trained PPO policy when target angle of attack of  $0.52 \text{ rad}$  ( $30^\circ$ )  
 (a) velocity ( $V$ ) ( $\text{ft/sec}$ ) (b) angle of attack ( $\alpha$ ) ( $\text{rad}$ ) (c) angle of sideslip ( $\beta$ ) ( $\text{rad}$ ).

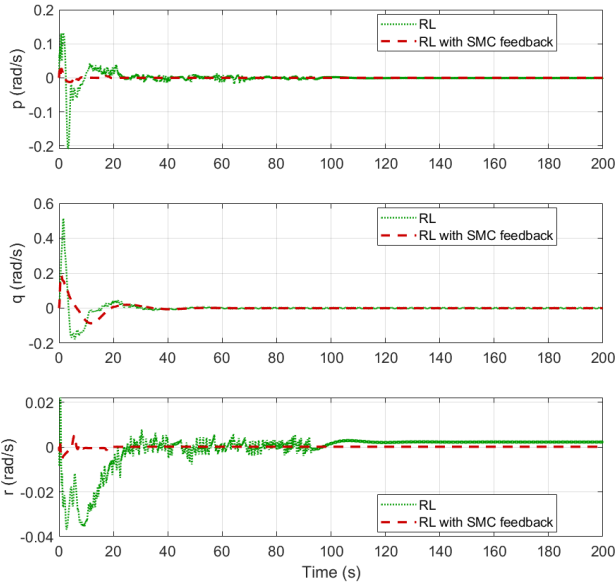


Fig. 13. System response for a partially trained PPO policy when target angle of attack of 0.52 rad (30°)  
 (a) roll rate ( $p$ ) (rad/sec) (b) pitch rate ( $q$ ) (rad/sec) (c) yaw rate ( $r$ ) (rad/sec).

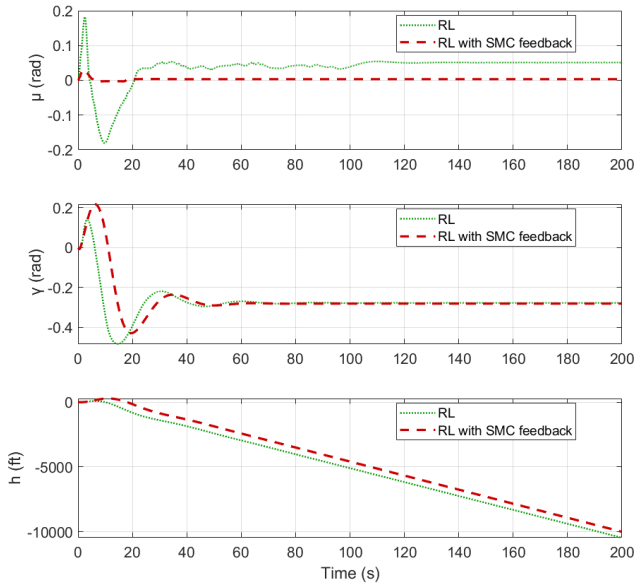


Fig. 14. System response for a partially trained PPO policy when target angle of attack of 0.52 rad (30°)  
 (a) bank angle ( $\beta$ ) (rad) (b) flight path angle ( $\gamma$ ) (rad) (c) altitude ( $h$ ) (ft).

Angle of sideslip again shows a little offset of 0.05 rad (less than 3°) in Fig. 12(c). However with a safety feedback of SMC feedback this also dies down. Yaw rate converge to small nonzero value in RL only simulation. It

is to be noted that these trained RL models are partially trained and still hold potential for improvement.

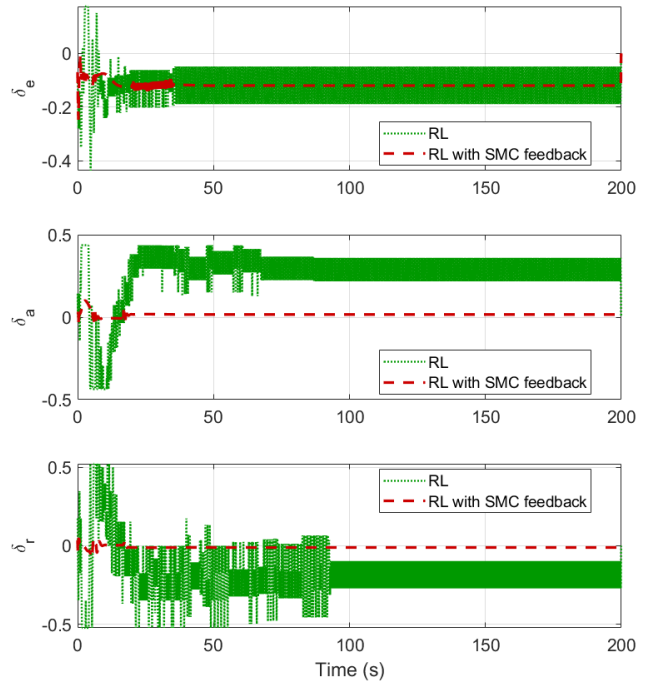


Fig. 15. Control surface deflection values generated by partially trained PPO policy when target angle of attack of 0.52 rad (30°)  
 (a) elevator ( $\delta_e$ ) (rad) (b) aileron ( $\delta_a$ ) (rad) (c) rudder ( $\delta_r$ ) (rad).

It can be observed from these two simulations that the safety layer suppresses destabilizing control deflections without noticeably impeding beneficial learned responses, provided the RL action lies within safe bounds.

Even with incomplete training, the hybrid scheme can salvage and enhance policy performance by enforcing stability envelopes, making it a viable intermediate step in the deployment pipeline when full training is ongoing.

### C. Fully Trained RL Model Simulation: RL vs. SMC vs. RL with SMC feedback

In the second phase, the RL policy was fully trained for spin recovery over 120 million timesteps, with domain randomization across mass, aerodynamic coefficients, and wind disturbances. The training objective combined the two-phase reward described in Section IV-A with potential-based reward shaping to promote rapid rate damping followed by attitude stabilization. The aircraft was allowed to remain in spin for first 30 seconds of simulation on purpose to demonstrate the spin condition. After this interval, controller was allowed to take up the recovery task. This is done to demonstrate the aircraft behavior in the spin condition for first 30 seconds. The network architecture is an Actor-Critic Network of [256, 128] hidden layers - Tanh configuration each. Learning

rate and Discount factor were kept at  $5e-5$  and  $0.99$  to encourage smooth learning and long-term rewards. The control authority factor is set to  $\zeta = 1$  when  $|e_\alpha|$ ,  $|e_\beta|$ , or  $|e_\mu|$  exceed  $0.05$ , while inside this bounded error tube the sliding-mode feedback is relaxed, allowing the reinforcement-learning feedforward policy to dominate the control action within certified bounds.

We do comparison of three controllers:

- **RL-only** — fully trained PPO policy.
- **SMC-only** — pure robust feedback law without learned feedforward.
- **RL control with SMC feedback** — fully trained PPO policy with SMC feedback and the safety filter.

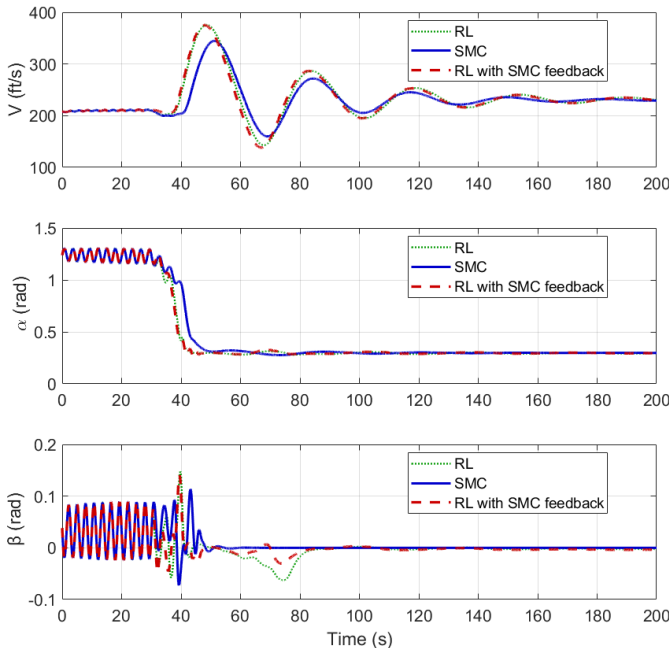


Fig. 16. System response of an aircraft under spin recovery using a trained PPO policy.

(a) velocity ( $V$ ) (ft/sec) (b) angle of attack ( $\alpha$ ) (rad) (c) angle of sideslip ( $\beta$ ) (rad).

Figs. 16–19 reveal the following trends:

In Fig. 16, The RL-only controller achieves the shortest recovery to the desired angle of attack  $\alpha_d$ , followed closely by the RL–SMC hybrid controller. The difference in recovery time is negligible, as the hybrid scheme exhibits similar convergence behavior with oscillations of negligible amplitude.

There is a significant delay of around 8-10 seconds for SMC as seen in Fig. 16(b). From Fig. 16 RL with SMC produces least overshoots in angle of sideslip and even in velocity and flight path angle which is not directly being controlled. The RL controller achieves rapid trajectory tracking but displays mild oscillatory behavior in  $\mu$ . The RL–SMC hybrid controller exhibits the small deviations

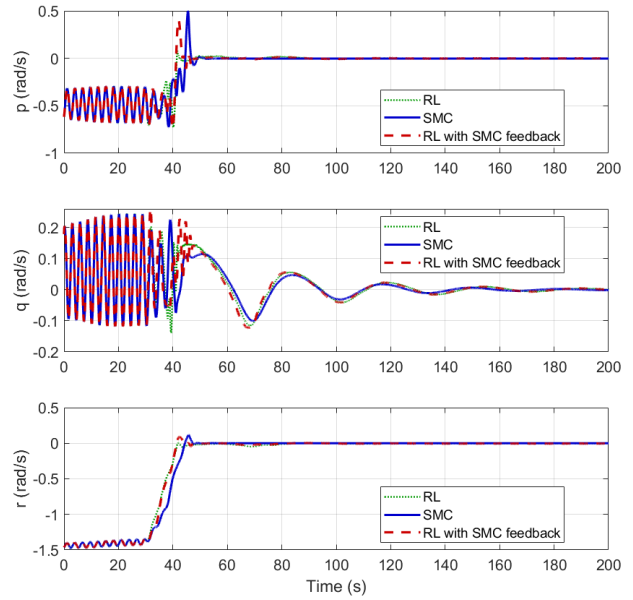


Fig. 17. System response for a trained PPO policy aircraft undergoing spin recovery

(a) roll rate ( $p$ ) (rad/sec) (b) pitch rate ( $q$ ) (rad/sec) (c) yaw rate ( $r$ ) (rad/sec).

in  $\mu$ ; however, its overall behavior lies between that of the RL-only and SMC controllers.

In the fully trained model, it can be observed that the RL controller gives the best performance when the model has been properly trained as shown in Fig. 19. However the control inputs produced are chattered and to train a RL model to produce controls with chattering can be very expensive computationally as it will require more training [18], [32]. It is also worth mentioning that even if such training is feasible it can pose the risk of overfitting phenomenon. SMC controller can be seen as an effective but a conservative controller which provides robustness and safety guarantees, something that RL model even though trained sufficiently may still lack [33]. RL feedforward control with SMC feedback filter produces inputs with significant reduction in chattering as well gives comparitely better performance that has faster tracking as well as safety guarantees because of its hybrid architecture.

*Interpretation:* In the partially trained models, the hybrid architecture consistently outperforms individual controllers by leveraging the anticipatory, coupling-aware commands from RL while maintaining the constraint-respecting stability properties of SMC. The safety filter ensures that, even in off-nominal conditions, the RL term cannot destabilize the system, while the SMC term rapidly corrects any deviation. With fully trained RL model, the proposed hybrid architecture gives optimal performance as the safety layer regularizes commands, lowers total variation and chatter while retaining the coordinated char-

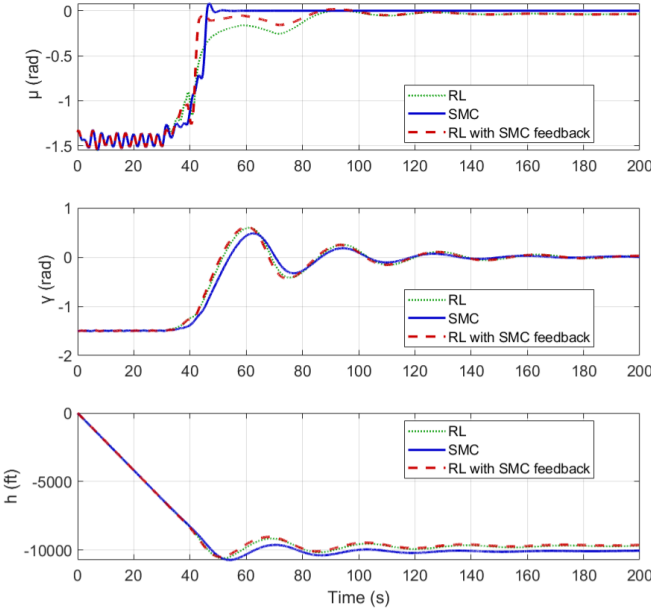


Fig. 18. System response for a trained PPO policy aircraft undergoing spin recovery

(a) bank angle ( $\beta$ ) (rad) (b) flight path angle ( $\gamma$ ) (rad) (c) altitude ( $h$ ) (ft).

acter of the learned policy. One key aspect in which the RL controller outperforms the other approaches is its anticipatory nature, which motivates the use of RL as a feedforward control component. In contrast, the SMC controller is inherently reactive, and its corrective action is therefore slightly delayed when compared with the RL-based policy. The proposed hybrid architecture achieves both the anticipatory behavior of RL as well as stability guarantees of SMC. This necessitates careful tuning of the control authority of the SMC feedback term, denoted by  $\zeta$ .

#### D. Key Insights

The following key insights are observed from the results.

- RL is an anticipatory controller so its response is much faster than SMC controller which is a reactive controller.
- Even partially trained RL policies benefit markedly from the SMC safety layer, which stabilizes residual oscillations and bounds overshoot without completely overriding useful learned behavior.
- The safety-filtered design ensures robustness to modelling errors and disturbances, enabling wider envelope application without retraining.
- The ability to operate with partial RL policies under SMC safety constraints provides a practical road

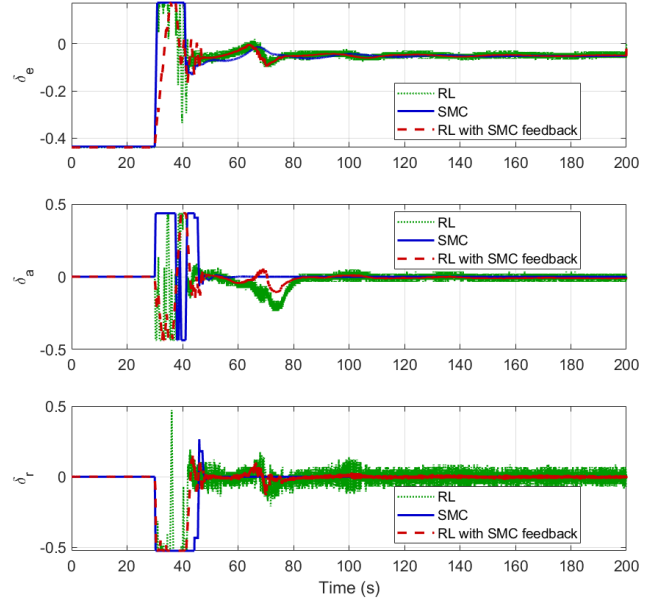


Fig. 19. Control surface deflection values generated by a trained PPO policy aircraft undergoing spin recovery

(a) elevator ( $\delta_e$ ) (rad) (b) aileron ( $\delta_a$ ) (rad) (c) rudder ( $\delta_r$ ) (rad).

map for incremental deployment in safety-critical domains.

- Actuator usage with RL-only is aggressive and noisy; SMC and RL-SMC hybrid substantially reduce the actuator total variation, and high-frequency chatter.
- The hybrid control architecture preserves the anticipatory benefits of RL while enforcing SMC-style stability and constraint compliance, providing the best possible trade-off for flight-critical use.

## VII. CONCLUSION

This work develops and evaluates a learning-augmented flight-control architecture that combines a deep reinforcement learning policy in the feedforward path with a sliding-mode controller in feedback, guarded by a supervisory safety filter on surface deflections and rates. Unlike prior learning-augmented control frameworks, this work provides an explicit control-theoretic integration of reinforcement learning and sliding-mode control through a bounded feedforward formulation. The learned policy is modeled as a matched, norm-bounded input, and a tunable control authority factor is introduced to regulate the dominance of the robust feedback law. A Lyapunov-based analysis establishes a direct relationship between admissible learning error, disturbance magnitude, and sliding-mode gain selection, yielding a certified invariant neighborhood under actuator saturation.

Across upset-recovery trials on the F-18/HARV model, the hybrid controller consistently delivered the

best overall trade-off. It preserved the anticipatory behavior of the learned policy while enforcing stability and hard actuator constraints, thereby reducing overshoot, residual oscillations, and control chatter relative to either RL-only or SMC-only baselines. Notably, even partially trained policies became reliably usable when wrapped with the SMC safety layer, and fully trained policies benefited from regularization that lowered total variation in the commands without erasing coordinated responses.

Methodologically, the paper contributes a simple integration recipe that is implementation-ready: (i) a two-phase, PBRS-based reward that first damps rates and then tightens attitude tracking, (ii) an SMC design that supplies robustness to modeling errors and disturbances, and (iii) a lightweight safety filter that caps learned authority and enforces deflection and rate limits. A Lyapunov-style analysis clarifies how the feedback layer counteracts residual feedforward errors from the policy.

There are limitations as the results are simulation-based, actuator dynamics are simplified, and tuning choices for gains and safety limits were empirical. Future work will migrate the architecture to hardware-in-the-loop, incorporate explicit actuator and sensor dynamics, and investigate adaptive or reference-governor style scheduling of SMC gains and safety limits. Overall, the study shows that combining learned feedforward with robust sliding-mode feedback and explicit constraint handling is a practical path to bring modern learning into safety-critical flight control.

## REFERENCES

- [1] S. Bhasin, N. Sharma, P. Patre, and W. Dixon, “Asymptotic tracking by a reinforcement learning-based adaptive critic controller,” *Journal of Control Theory and Applications*, vol. 9, pp. 400–409, 08 2011.
- [2] X. Hao, Z. Xin, W. Huang, S. Wan, G. Qiu, T. Wang, and Z. Wang, “Deep reinforcement learning enhanced pid control for hydraulic servo systems in injection molding machines,” *Scientific Reports*, vol. 15, p. 23005, 07 2025.
- [3] J. Sierra-García *et al.*, “Wind turbine pitch reinforcement learning control improved by pid regulator and learning observer,” *Engineering Applications of Artificial Intelligence*, vol. 111, p. 104769, 2022.
- [4] D. Baek *et al.*, “Hybrid lmc: Hybrid learning and model-based control for wheeled humanoid robot via ensemble deep reinforcement learning,” *arXiv preprint arXiv:2204.03159*, 2022.
- [5] M. Zanon and S. Gros, “Safe reinforcement learning using robust mpc,” *arXiv preprint arXiv:1906.04005*, 2020.
- [6] P. Dao and Y. Liu, “Adaptive reinforcement learning strategy with sliding mode control for unknown and disturbed wheeled inverted pendulum,” *International Journal of Control, Automation and Systems*, vol. 19, pp. 1139–1150, 2021.
- [7] H. van Hoof *et al.*, “Reinforcement learning with model-based feedforward inputs for robotic table tennis,” *Autonomous Robots*, 2023.
- [8] I. Sayyed, A. Konar, and N. K. Sinha, “Deep reinforcement learning based control design for aircraft recovery from loss-of-control scenario,” 2026. [Online]. Available: <https://arxiv.org/abs/2601.06439>
- [9] R. S. Sutton and A. G. Barto, *Reinforcement Learning: An Introduction*, 2nd ed. Cambridge, MA: MIT Press, 2018.
- [10] I. Stough, H. P., D. J. DiCarlo, and J. Patton, J. M., “Flight investigation of stall, spin and recovery characteristics of a low-wing, single-engine, t-tail light airplane,” NASA Langley Research Center, Hampton, VA, NASA Technical Publication NASA-TP-2427, May 1985, accession No. 85N25248. [Online]. Available: <https://ntrs.nasa.gov/citations/19850016937>
- [11] M. A. Croom *et al.*, “Spin resistance and post-stall flight research,” NASA Langley Research Center, Hampton, VA, NASA Technical Memorandum NASA-TM-107769, 1993, g. Croom *et al.*
- [12] A. Khatri, J. Singh, and N. Sinha, “Aircraft maneuver design using bifurcation analysis and sliding mode control techniques,” *Journal of Guidance, Control, and Dynamics*, vol. 35, pp. 1435–1449, 09 2012.
- [13] J. Schulman, F. Wolski, P. Dhariwal, A. Radford, and O. Klimov, “Proximal policy optimization algorithms,” 2017.
- [14] J. García and F. Fernández, “A comprehensive survey on safe reinforcement learning,” *Journal of Machine Learning Research*, vol. 16, pp. 1437–1480, 2015.
- [15] R. Bellman, R. Bellman, and R. Corporation, *Dynamic Programming*, ser. Rand Corporation research study. Princeton University Press, 1957. [Online]. Available: <https://books.google.co.in/books?id=rZW4ugAACAAJ>
- [16] T. P. Lillicrap, J. J. Hunt, A. Pritzel, N. Heess, T. Erez, Y. Tassa, D. Silver, and D. Wierstra, “Continuous control with deep reinforcement learning,” 2016.
- [17] J. Schulman, S. Levine, P. Abbeel, M. I. Jordan, and P. Moritz, “Trust region policy optimization,” 2015.
- [18] H. Lee and V. I. Utkin, “Chattering suppression methods in sliding mode control systems,” *Annual reviews in control*, vol. 31, no. 2, pp. 179–188, 2007.
- [19] C. Xiu and P. Guo, “Global terminal sliding mode control with the quick reaching law and its application,” *IEEE Access*, vol. 6, pp. 49 793–49 800, 2018.
- [20] S. Singh, “Asymptotically decoupled discontinuous control of systems and nonlinear aircraft maneuver,” *IEEE Transactions on Aerospace and Electronic Systems*, vol. 25, no. 3, pp. 380–391, 1989.
- [21] S. H. Lane and R. F. Stengel, “Flight control design using non-linear inverse dynamics,” *Automatica*, vol. 24, no. 4, pp. 471–483, 1988. [Online]. Available: <https://www.sciencedirect.com/science/article/pii/0005109888900921>
- [22] I. Sayyed, “Adaptive gain regulation and modulation for robust asymptotic stability in nonlinear systems with input saturation,” in *2024 6th International Conference on Control and Robotics (ICCR)*, 2024, pp. 46–55.
- [23] J.-J. E. Slotine, W. Li *et al.*, *Applied nonlinear control*. Prentice hall Englewood Cliffs, NJ, 1991, vol. 199, no. 1.
- [24] D. Kim, G. Oh, Y. Seo, and Y. Kim, “Reinforcement learning-based optimal flat spin recovery for unmanned aerial vehicle,” *Journal of Guidance, Control, and Dynamics*, vol. 40, no. 4, pp. 1076–1084, 2017.
- [25] A. Y. Ng, D. Harada, and S. Russell, “Policy invariance under reward transformations: Theory and application to reward shaping,” in *Proceedings of the 16th International Conference on Machine Learning (ICML)*, 1999, pp. 278–287.
- [26] G. Brockman, V. Cheung, L. Pettersson, J. Schneider, J. Schulman, J. Tang, and W. Zaremba, “Openai gym,” 2016.
- [27] A. Raffin, A. Hill, A. Gleave, A. Kanervisto, M. Ernestus, and N. Dormann, “Stable-baselines3: Reliable reinforcement learning implementations,” *Journal of Machine Learning Research*, vol. 22, no. 268, pp. 1–8, 2021. [Online]. Available: <http://jmlr.org/papers/v22/20-1364.html>
- [28] J. Song, Y. Niu, and Y. Zou, “Finite-time stabilization via sliding mode control,” *IEEE Transactions on Automatic Control*, vol. 62, no. 3, pp. 1478–1483, 2016.
- [29] X. Yu, Y. Feng, and Z. Man, “Terminal sliding mode control – an overview,” *IEEE Open Journal of the Industrial Electronics Society*, vol. 2, pp. 36–52, 2021.

[30] T. Hu and Z. Lin, *Control systems with actuator saturation: analysis and design*. Springer Science & Business Media, 2001.

[31] Y.-S. Zhong, “Globally stable adaptive system design for minimum phase siso plants with input saturation,” *Automatica*, vol. 41, no. 9, pp. 1539–1547, 2005.

[32] H. U. Suleiman, M. B. Mu’azu, T. A. Zarma, A. T. Salawudeen, S. Thomas, and A. A. Galadima, “Methods of chattering reduction in sliding mode control: A case study of ball and plate system,” in *2018 IEEE 7th International Conference on Adaptive Science & Technology (ICAST)*, 2018, pp. 1–8.

[33] D. M. K. K. V. Rao and N. K. Sinha, “Aircraft spin recovery using a sliding-mode controller,” *Journal of Guidance, Control, and Dynamics*, vol. 33, no. 5, pp. 1675–1679, 2010. [Online]. Available: <https://doi.org/10.2514/1.50186>

PLACE  
PHOTO  
HERE

**Imran Sayyed** received the Bachelor’s degree in Mechanical Engineering from Panjab University and is currently pursuing the M.S. degree in the Flight Mechanics and Control Laboratory at the Indian Institute of Technology Madras, Chennai, India.

His research focuses on nonlinear and adaptive control of aircraft, with emphasis on sliding mode control, reinforcement learning-based flight control, and six-degree-of-freedom flight dynamics modeling. His work involves developing robust controllers for spin recovery and integrating model-based and data-driven approaches for flight envelope protection.

PLACE  
PHOTO  
HERE

**Dr. Nandan Kumar Sinha** is a professor in the Department of Aerospace Engineering at IIT Madras since 2014. Dr. Sinha has BTech, MTech, and PhD degrees in Aerospace Engineering from IITs Bombay and Kanpur. He was a visiting post-doctoral scholar at the TU-Darmstadt, Germany prior to joining IIT Madras as faculty in 2006.

His expertise lies in the areas of Dynamics and Control of Aerospace Vehicles. Dr. Sinha has co-authored two books “Elementary Flight Dynamics with an Introduction to Bifurcation and Continuation Methods (Ed 1, 2013; Ed 2, 2022)” and “Advanced Flight Dynamics with Elements of Flight Control (2017)” with Dr. N Ananthkrishnan. Dr. Sinha has also made video- and web- lecture series on the topics of Aircraft Flight Dynamics and Satellite Technology under the aegis of NPTEL.

Dr. Sinha was a nominee and participant of the IVLP (International Visitor Leadership Program) of the Department of State, USA in 2018. Dr. Sinha serves as an expert member on many committees, both in academia and in industry.